Brain Topography (2018) 31:848–862
https://doi.org/10.1007/s10548-018-0643-x

ORIGINAL PAPER

Consciousness Indexing and Outcome Prediction with Resting-State EEG in Severe Disorders of Consciousness

Sabina Stefan[1] · Barbara Schorr[2,3] · Alex Lopez-Rolon[4] · Iris-Tatjana Kolassa[3] · Jonathan P. Shock[5] · Martin Rosenfelder[2,3] · Suzette Heck[4] · Andreas Bender[2,4]

Received: 30 May 2017 / Accepted: 7 April 2018 / Published online: 17 April 2018

Abstract

We applied the following methods to resting-state EEG data from patients with disorders of consciousness (DOC) for consciousness indexing and outcome prediction: microstates, entropy (i.e. approximate, permutation), power in alpha and delta frequency bands, and connectivity (i.e. weighted symbolic mutual information, symbolic transfer entropy, complex network analysis). Patients with unresponsive wakefulness syndrome (UWS) and patients in a minimally conscious state (MCS) were classified into these two categories by fitting and testing a generalised linear model. We aimed subsequently to develop an automated system for outcome prediction in severe DOC by selecting an optimal subset of features using sequential floating forward selection (SFFS). The two outcome categories were defined as UWS or dead, and MCS or emerged from MCS. Percentage of time spent in microstate D in the alpha frequency band performed best at distinguishing MCS from UWS patients. The average clustering coefficient obtained from thresholding beta coherence performed best at predicting outcome. The optimal subset of features selected with SFFS consisted of the frequency of microstate A in the 2–20 Hz frequency band, path length obtained from thresholding alpha coherence, and average path length obtained from thresholding alpha coherence. Combining these features seemed to afford high prediction power. Python and MATLAB toolboxes for the above calculations are freely available under the GNU public license for non-commercial use (https://qeeg.wordpress.com)

Keywords Quantitative EEG · Unresponsive wakefulness syndrome · Minimally conscious state · Outcome prediction · Microstate analysis · Sequential floating forward selection

Introduction

Severe disorders of consciousness (DOC) are states of unconsciousness caused by injury or malfunction of neural systems which regulate arousal and awareness (Posner et al. 2007; Giacino et al. 2014). Despite significant advances in medical technology, patients with DOC may remain in a vegetative state, also known as unresponsiveness wakefulness syndrome (UWS), characterised by arousal without awareness (Laureys et al. 2010), or a minimally conscious state (MCS), defined by definite but minimal behavioural signs of awareness of oneself and one's environment, which may wax and wane (Giacino et al. 2002). For ethical, therapeutic and economic reasons, it is important to predict outcome as early, reliably and sensitively as possible (Graf et al. 2008; Grill et al. 2013; Lopez-Rolon et al. 2015).

The best criterion available to date for establishing the diagnosis of UWS or MCS is behavioural assessment by means of the clinical scales such as the revised version of

Handling Editor: Christoph M. Michel.

Electronic supplementary material The online version of this article (https://doi.org/10.1007/s10548-018-0643-x) contains supplementary material, which is available to authorized users.

✉ Jonathan P. Shock
jonathan.shock@uct.ac.za

[1] School of Engineering, Brown University, 182 Hope Street, Box D, Providence, RI 02912, USA

[2] Department of Neurology, Therapiezentrum Burgau, Kapuzinerstrasse 34, 89331 Burgau, Germany

[3] Clinical and Biological Psychology, Institute of Psychology and Education, Ulm University, 89081 Ulm, Germany

[4] Department of Neurology, University of Munich, Marchioninistrasse 15, 81377 Munich, Germany

[5] Department of Mathematics and Applied Mathematics, University of Cape Town, Rondebosch, Private Bag X1, Cape Town 7701, South Africa

the coma recovery scale (CRS-R). However, although every effort is made in clinical settings to avoid it, patients who do understand CSR-R commands, but are unable to follow them due to motor impairments could potentially receive a wrong UWS diagnosis.

Finding more accurate methods for discriminating DOC diagnostic groups is imperative, considering that diagnosis has a direct impact on decisions regarding life-sustaining therapy (Howell et al. 2013), and misdiagnosis prevalence has been reported to be possibly as high as 43% (Howell et al. 2013).

Electroencephalography (EEG) is a non-invasive, safe and relatively easy method for gauging the function of the brain, which allows the application of quantitative methods to better understand and interpret patterns of EEG data related to DOC (Kondziella et al. 2016). Applied to DOC, as expected these methods are focussed on the objective assessment of EEG signals and aim to detect subtleties that may escape visual inspection, thus minimising subjectivity and human error in prognostication (Schorr et al. 2015, 2016). Thus, these methods may expand the manner in which EEG is currently used in clinical practice by providing a more rigorous, objective and statistically coherent analysis of the data through the mathematical extraction of descriptive parameters (Gosseries et al. 2011). High-density EEG techniques in particular are a promising avenue of research, which is playing increasingly an important role in diagnosis and prognosis (Noirhomme and Laureys 2014).

However, researchers are still to find EEG features, which could index consciousness in such a manner as to be able to substitute reliably behavioural assessment in diagnosis and outcome prediction, where outcome categories are defined here as UWS or dead, and MCS or better.

In the present exploratory study we applied to resting-state, high-density EEG data from patients with DOC the following methods to examine the extent to which they could be used for consciousness indexing and outcome prediction: microstates, entropy (i.e. approximate, permutation), power in alpha and delta frequency bands, and connectivity (i.e. weighted symbolic mutual information, symbolic transfer entropy, complex network analysis). These are techniques that are commonly applied in EEG studies, but it remains unclear the relative performance of each metric in assessing consciousness. The aim then is to be able to assess these measures on a single dataset as well as apply and evaluate EEG measures that aren't ordinarily applied in DOC studies. This allows us then to apply machine-learning techniques to build a model to predict coma outcome, which may be a viable method to provide information on an individual basis, as opposed to group differences, as often done in DOC studies (Noirhomme et al. 2015).

To build the model, we extracted an optimal subset of features using sequential forward floating selection (SFFS), which is an algorithm selects a subset of EEG features by starting from an empty set and adding incrementally one feature at a time and deleting them conditionally while avoiding partially the local optima of the correct classification rate (Ververidis and Kotropoulos 2008).

The present exploratory study used standardized clinical evaluations at baseline and follow-up by means of the CRS-R to minimize misdiagnosis, which could also influence the analysis of EEG features. As noted in the review by Noirhomme et al. considerable limitations of machine-learning applied to EEG is the difficulty in establishing a reliable behavioural assessment and fluctuations in the patient's level of arousal (Noirhomme et al. 2015). In the absence of a gold standard to assess consciousness, consilience between multiple independent assessments might be a rational way forward as applied in the study by Chennu et al. (2017). In this study, the authors compared EEG measures to results obtained from positron emission tomography, which may be a useful method of validating EEG studies. Another important consideration is the sample size needed in such machine-learning studies to ensure robustness and generalizability of results—for example, in the review by Noirhomme et al., they only consider studies with over 50 patients, but it remains unclear whether that is sufficient. However, it may still be illuminating as a starting point to observe how various biomarkers compare on a small sample size.

We must also note that we do not aim to address known limitations of the techniques evaluated in this study, but to investigate several EEG biomarkers of consciousness on the same dataset to be able to compare the relative usefulness of these features. We also aimed to apply measures that are ordinarily applied to index consciousness to instead predict outcome, thus avoiding the complication of assessing prognosis through diagnosis.

Microstate Analysis

Microstate analysis is a spatio-temporal method that analyses the topographical maps of electrical potentials over the electrode array as well as the temporal evolution of these topographies, such that multichannel EEG data is essentially considered as a series of sequential topographies of electric fields (Pascual-Marqui et al. 1995). Interestingly, most studies find that four archetypal maps account for over 70% of total topographical variance, and furthermore that EEG topography remains quasi-stable for about 80–120 ms before abruptly changing into a topography represented by a different archetypal map (Murray et al. 2008). Microstates are thus defined as these archetypal maps of quasi-stability, during which global topography is invariant, although electric field strength may vary and polarity invert (Lehmann et al. 1987). The four topographies that are the most commonly exhibited are,

A right-frontal to left-posterior
B left-frontal to right-posterior
C frontal to occipital
D mostly frontal and medial to slightly less occipital activity than class C

It has been suggested that microstates reflect primitive information processing such that their generation is likely the result of the activity of distinct neural arrays associated with specific neural functions (Lehmann et al. 1998). Microstate analyses have proven to be useful in classifying transitive brain states. For example, it has been shown that microstate B in schizophrenics displays significantly different field configurations and shorter durations in patients than controls (Lehmann et al. 2005). Furthermore, microstate analyses have been applied to investigate differences in sleep stages between narcoleptic patients and controls and to probe the brain in different sleep stages (Kuhn et al. 2015; Brodbeck et al. 2012). This is a promising avenue of research considering that microstate analyses have been successful in probing the brain in different states, potentially allowing for the discrimination of patients in UWS/MCS states. Furthermore, such analyses might help us to understand key differences in the brain functions of patients with different severities of coma. As far as we know, microstate analyses have not previously been employed in this manner for the investigation of DOC and DOC outcome prediction, and may be an interesting topic of future research. In this paper, however, we do not intend to make biological claims between DOC patients in different outcome groups, but rather assess how predicative this common EEG technique in assessing consciousness as well as coma outcome.

Entropy

Measures of entropy applied to EEG signals aim to quantify the unpredictability of outputs of the complex system of neural networks underlying consciousness. Numerous measures of entropy have been applied to the analysis of EEG signals, particularly in the studies of anesthesia and epilepsy (Bruhn et al. 2000; Kannathal et al. 2005). However, measures of entropy, such as approximate entropy (ApEn) and permutation entropy specifically, are increasingly being investigated with relation to coma and consciousness, with some interesting preliminary results. For example, Sarà et al. have shown a correlation between *ApEn* measures and outcome of patients with UWS (Sarà et al. 2011), although Gosseries et al. found entropy to only be useful in diagnosis, and not prognosis (Gosseries et al. 2011). The present study extends the work of previous studies in analysing *ApEn* as a predictor of DOC outcome, and also investigates the prognostic value of permutation entropy as explored for the first time, as far as we know. These measures of entropy are potentially useful because they are scale-invariant, robust to noise, and discriminate series for which clear feature recognition is difficult (Pincus 1995; Pincus and Singer 2014).

Approximate Entropy

Conceptually, approximate entropy (*ApEn*) is defined as the logarithmic likelihood that the patterns of data that are close to each other will remain close on following, incremental comparisons. Mathematically, *ApEn* is determined as follows: Given a segment of EEG of N time samples, $[u(1), u(2), \ldots, u(N)]$, and an arbitrary value m, a sequence of vectors $[x(1), x(2), \ldots, x(N-m+1)]$ in m-dimensional space can be constructed such that $x(i) = [u(i), u(i+1), \ldots, u(i+m-1)]$. Using $x(i)$, and additional quantity, $C^m{}_i$, can be calculated:

$$C^m{}_i(r) = \frac{\text{number of } x(j) \text{ such that } |x(i) - x(j)| < r}{N - m + 1} \tag{1}$$

where r is an arbitrary tolerance. This can be used to define

$$\phi^m(r) = \frac{1}{N-m+1} \sum_{i=1}^{N-m+1} \log(C^m{}_i(r)) \tag{2}$$

such that

$$ApEn = \phi^m(r) - \phi^{m+1}(r) \tag{3}$$

Permutation Entropy

In contrast to *ApEn*, permutation entropy (*PerEn*) makes use of the symbolic transform, such that the signal is represented by a sequence of discrete symbols, the probability density of which is analysed to obtain the entropy. Symbolization of EEG data is a useful practice because it reduces sensitivity to noise, simplifies computational evaluations, and consequently increases efficiency in quantifying information from a complex dynamical system (Daw et al. 2003). The transformation involves the extraction of sub-vectors of the signal, like in the case of ApEn, each composed of voltages at m time points separated by a fixed time delay, τ . For example, given a segment of EEG of N time samples, $[u(1), u(2), \ldots, u(N)]$, a set of subvectors can be constructed, $[x(1), x(2), \ldots, x(N-m+1)]$, where a subvector is defined as $x(i) = [u(i), u(i+\tau), \ldots, u(i+(m-1) \times \tau)]$. Each $x(i)$ is then represented by a symbol (or equivalently a number between 1 and m!) dependent on the order of amplitudes of the signal which comprise the subvector. Permutation entropy can then be calculated as,

$$PerEn = -\sum_{i=1}^{m!} p_i \log(p_i) \tag{4}$$

where p_i is the probability of occurrence of the ith symbol.

Power in Alpha and Delta Frequency Bands

Some studies have shown that differences in power spectra exist between patients with DOC and healthy controls, as well as between UWS and MCS patients (Lehmann et al. 1987; Blume et al. 2015; Stender et al. 2015). In particular, these studies have indicated that patients with DOC exhibit reduced power in the alpha band and increased power in the delta band, with a more severe difference presented in the UWS than the MCS. We verified these results by establishing how accurately power in these bands differentiate patients in the UWS and MCS, and furthermore we determine the effectiveness of using spectral power in these frequency bands to prognosticate in DOC.

Connectivity

Previous research has been done into comparing the brain connectivity of UWS and MCS through indices such as coherence, the imaginary part of coherence, weighted symbolic mutual information and symbolic transfer entropy, all of which are further explored in this study (Lehembre et al. 2012; King et al. 2013; Lee et al. 2015). These indices provide insight into the degree of integration and connection of networks in the brain by assessing connectivity between electrode signals. Previous research tend to agree that patients in UWS display significantly lower connectivity than MCS patients in the theta and alpha bands, indicating that the level of connectivity could be related to the severity of the disorder. Connectivity is likely to correlate to greater brain activity in terms of information sharing and processing, and therefore also to behavioural signs of consciousness, thus warranting further investigation in this area.

Coherence

Coherence quantifies the degree of coupling of frequency spectra between two electrodes, and can be calculated for a frequency f as,

$$C_{xy}(f) = \frac{|G_{xy}(f)|^2}{G_{xx}(f)G_{yy}(f)} \tag{5}$$

where $G_{xy}(f)$ is the cross-spectral density of x and y, where x and y are time-series of voltages recorded at different electrodes, and $G_{xx}(f)$ and $G_{yy}(f)$ are the auto-spectral densities of x and y respectively. Coherence has the significant disadvantage of being contaminated by volume conduction, which is the transmission of electrical signals from a primary source through brain tissue (Nunez et al. 1997). To overcome this issue, and thereby provide a more accurate reflection of brain interactions, one approach is to consider only the imaginary part of coherence since volume conduction only affects the real part of coherence. It is not necessarily the intention of this paper to correct the shortcomings or address the limitations of techniques applied in EEG research, but rather investigate techniques that are commonly applied in EEG research. This paper thus considers both magnitude-squared coherence as well as imaginary coherence the both are measures often justified by EEG researchers. We also note that the position of the reference electrode affect the possible network topologies generated, but we do not intend to make claims about the absolute values of coherence, but rather differences between patients groups (for which the reference electrode was located at the vertex for all patients).

Weighted Symbolic Mutual Information

Weighted symbolic mutual information (*wSMI*) is based on principles of permutation entropy applied to the quantification of global information sharing (King et al. 2013). Once having symbolically-transformed the signal as in the case for permutation entropy, the method assesses the joint occurrences of symbolic or qualitative fluctuations in the signal, thus robustly detecting non-directional nonlinear coupling. To account for spurious correlations produced by artifacts (such as those from volume conduction), wSMI disregards trivial conjunctions of symbols across two signals, corresponding to conjunctions of identical symbols, as well as conjunctions of opposite symbols. This is achieved by attributing a zero weight to symbol pairs as indicated on the joint probability matrix illustrated in Fig. 1.

wSMI can then be calculated as,

$$wSMI(\hat{X}, \hat{Y}) = \frac{1}{\log(k!)} \sum_{\hat{x}\in\hat{X}} \sum_{\hat{y}\in\hat{Y}} w(\hat{x},\hat{y}) p(\hat{x},\hat{y}) \log \frac{p(\hat{x},\hat{y})}{p(\hat{x})p(\hat{y})} \tag{6}$$

where $\hat{x}$ and $\hat{y}$ are symbols present in signals $\hat{X}$ and $\hat{Y}$ respectively, $p(\hat{x},\hat{y})$ is the joint probability of co-occurrence of $\hat{x}$ and $\hat{y}$, $p(\hat{x})$ and $p(\hat{y})$ are the probabilities of $\hat{x}$ and $\hat{y}$ in $\hat{X}$ and $\hat{Y}$, respectively. Lastly, $w(\hat{x},\hat{y})$ represents the weights (0 or 1) as described in Fig. 1. The reasoning behind the zero-weighting is that conjunctions of identical symbols may be elicited by a common source, and conjunctions of opposite symbols may reflect opposite sides of a common electric dipole.

Symbolic Transfer Entropy

Transfer entropy (*TE*) quantifies the directional transfer of information by assessing the uncertainty of the current value of voltage at one electrode position Y knowing past voltages at another position X compared to the uncertainty in the voltage at Y only knowing past voltages at Y. *TE* is based on

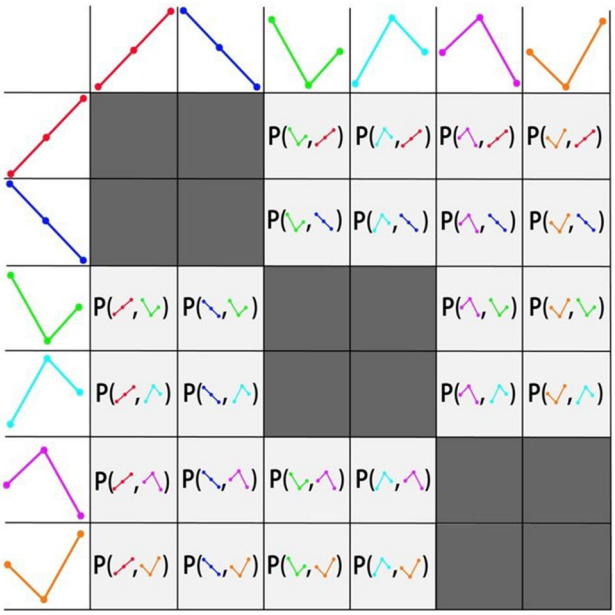

Fig. 1 The joint probability matrix for a symbol transformation with $m = 3$. Dark grey blocks are zero-weighted ($w = 0$) and do not contribute to the *wSMI*

Granger Causality, a linear regression model that quantifies the causal interaction between a source signal *X* and target signal *Y*:*X* is said to Granger-cause *Y* if the inclusion of the past of *X* improves the prediction of *Y* (Barnett et al. 2009) . *TE* thus differs from Granger Causality in that it is framed in terms of resolution of uncertainty, not in terms of prediction. However, it has been shown that *TE* is equivalent to Granger causality under Gaussian assumptions (Barnett et al. 2009). Granger Causality is known to produce spurious results due to its linearity, sensitivity to noise, and sensitivity to band-pass filtering. *TE* is a robust, nonlinear approach that was consequently introduced to address these limitations (Lee et al. 2015). However, we did not evaluate the possibility of spuriousness correlation with regards to *TE*, but instead employed this technique as is commonly performed in EEG research.

TE offers a model-free estimation of the direction and strength of connectivity between two signals, X and Y, and can be defined as the measure of mutual information between the past of *X*, (*XP*), and the future of *Y*, (*YF*), when the past of *Y*, (*YP*) is already known.

Mathematically,

$$TE_{X\rightarrow Y} = \sum P(Y_F, Y_P, X_P) \log \left[\frac{P(Y_f | Y_P, X_P)}{P(Y_F, Y_P)} \right] \quad (7)$$

TE can be quite complex to determine because of the difficulty in estimating probability density functions from finite, irregular data. Moreover, to do so, data is quantised into equally-spaced bins, and it has been shown that *TE* estimates are dependent on this arbitrary choice in bin-size. To overcome this, we investigated symbolic transfer entropy, which quantifies *TE* of symbolically transformed data without the need for binning or advanced estimators of the probability density function.

Complex Network Analysis

Measures of connectivity can be employed in complex network analysis which aims to represent complex systems as networks and extract meaningful information from the topologies of these networks. Complex network analysis may be a particularly insightful tool because it allows for the exploration of structural–functional connectivity relationships by defining functional connections with respect to the spatial map of the brain. In EEG analyses, networks can be constructed by considering the electrode positions as nodes and the links between nodes as functional connections, as quantified by measures described above. The topology of these networks can be assessed and compared through graph-theoretical measures, such as the clustering coefficient and characteristic path length. The clustering coefficient of a network can be computed by examining triplets, which are defined as three nodes with at least two links. Specifically, the clustering coefficient is defined as the number of closed triplets (groups of three nodes which are maximally interconnected) divided by the total number of triplets. The clustering coefficient is thus a micro-scale measure that provides an indication of clustered connectivity around individual nodes, which in turn is indicative of segregated neural processing. Conversely, characteristic path length provides insight into macro-scale functioning by quantifying functional integration: the ability to combine specialized information from distributed brain regions. Characteristic path length is defined as the average number of steps along the shortest paths for all possible pairs of nodes, where each path represents a potential route of information flow between two brain regions.

Complex network analyses applied to EEG analysis are beginning to gain interest with promising results. Chennu et al. calculated numerous graph theoretic statistics from EEG data including the clustering coefficient, path length, modularity, participation coefficient and network-level modular span and found that connectivity as assessed by these metrics correlated well with positron emission tomography (Chennu et al. 2017). Furthermore, they found that these networks correlate strongly with brain metabolism.

In EEG studies, a network topology can be created by thresholding measures of connectivity between electrodes, such that a link is said to exist between two electrodes if the connectivity between those two electrodes exceed a certain threshold. In the study by Chennu et al. graph-theoretic

statistics are calculated by thresholding debiased weighted phase lag index, but in the present study we threshold the coherence because of its prevalence in coma research. The position of the reference electrode affects the descriptions of connectivity between electrodes, and consequently also the network topologies generated, but we do not intend to make claims about the absolute values, but rather differences between patients groups (for which the reference electrode was located at the vertex for all patients).

Method

Selection of Participant Sample

After receiving approval from the local ethics committee, we recruited DOC patients consecutively during admission to same intensive inpatient neurorehabilitation center in the German state of Bavaria. Legal representatives of participants gave written informed consent. Patients were not under sedation during EEG recording. The resulting participant sample contains only data from patients, who were available for a follow-up on their consciousness level at or after discharge from neurorehabilitation. The state of consciousness both at baseline and follow-up was assessed with the CRS-R. Details on inclusion and exclusion criteria as well as other study protocol related information have been published elsewhere (Grill et al. 2013).

Procedure

Prior to recording 5 min of high-density resting state EEG for each patient, we assessed the level of consciousness of patients with the CRS-R. Patients were in the supine position with eyes closed. The standard CRS-R arousal facilitation protocol was used to maintain the patient in a state of arousal during EEG recording.

Data

Data consists of resting-state data recorded at a sampling rate of 1000 Hz with a 256 channel high-density geodesic sensor net with Net Amps 300 amplifier and Net Station 4.5. software (Electrical Geodesic Inc., Eugene, OR, USA). During recording, electrodes were referenced to the vertex and impedances were kept under 50 kΩ. Data were high-pass filtered at 0.1 Hz to eliminate slow drifts and subsequently segmented into trials of two seconds, such that all described analyses are performed on the same resting-state data of two seconds in duration. Trials with eye-movement artefacts exceeding 55 µV and eye-blinks artefacts exceeding 140 µV were automatically removed. To determine channel outliers, we examined the distributions of the maximum voltage difference across all channels in that trial. If a channel exhibited a maximum change that was greater than five standard deviations, that channel was removed from analysis in that trial. This resulted in at most one to two channels being excluded in a single trial. Each analysis described in this paper was performed using ten trials.

Statistical Analysis

We analysed data using both MATLAB Release 2014b (Mathworks, Sherborn, Massachusetts, USA) and Python. To determine the predictive power of the measures explored in this study, patients were classified into one of two groups (UWS or MCS for diagnosis and UWS or dead, and MCS or better for prognosis) by fitting a generalised linear model (GLM) on training data, and testing the model on test data. Additionally, to avoid over-fitting and circular analysis, a ten-fold stratified cross-validation scheme was implemented. The performance of the classifiers was then investigated using receiver operating characteristic (ROC) curves. The ROC curve illustrates the performance of a binary classifier by plotting the true positive rate (sensitivity) against the false positive rate (1—specificity) as the threshold is varied. The outputs of the GLM are thresholded at values ranging between 0 and 1, thus binarizing the output of the GLM. These binary outputs are then compared to the actual labels (UWS vs. MCS, or improved vs. unimproved) represented by 0 and 1 s, allowing for the calculation of specificity and sensitivity. Each threshold yields a pair of values (one value for specificity and one for sensitivity), corresponding to one point on the ROC curve.

We calculated the area under the curve (AUC) of ROC curves to determine which features exhibited significant differences across groups of patients. The area under the curve (AUC) of a ROC provides a measure of classification accuracy, such that an of 100% indicates perfect classification (there is some value of the threshold parameter for which there is both perfect sensitivity and specificity) and 50% indicates random classification. Significance of the AUC was established by randomly permuting the elements of feature vectors and comparing the results using the non-parametric Kruskal–Wallis test (Mason and Graham 2002).

Finally, to account for multiple comparisons, the false discovery rate was controlled by employing the Benjamini–Hochberg procedure at level = 0.05. The procedure is as follows: the p values, $p_1, \ldots, p_m$, corresponding to the null hypotheses (features tested), $H_1, \ldots, H_m$, are sorted in increasing order. Each p value is compared to the Benjamini–Hochberg critical value, $\frac{i}{m}\alpha$, where i is the rank and m is the number of hypotheses. The largest p value that is less than the critical value is considered to be significant, as well as all p values smaller than it. Adjusted p values are

calculated as raw p values multiplied by $\frac{m}{i}$, and are reported in this study as q values.

Microstate Analysis

We performed a microstate segmentation following a protocol employed in previous studies (Koenig and Melie-Garca 2010). Specifically, we transformed EEG data to the average-reference, calculated the global field power (GFP) for each trial, and extracted topographic maps at time points of GFP local maxima, which correspond to times of greatest signal-to-noise ratio. The GFP is the standard deviation of the voltages recorded at all channels at each time point, and can be calculated as,

$$GFP = \sqrt{\frac{\sum_{i=1}^{N}(u_i - \bar{u}_i)^2}{N}} \tag{8}$$

where u_i is the voltage at electrode i, $\bar{u}_i$ is the average voltage of all electrodes, and N is the number of electrodes.

These maps at GFP maxima are assimilated for all trials, and clustered into a predetermined number of clusters using both a modified k-means and a "topographical atomise and agglomerate hierarchical clustering" algorithm (Murray et al. 2008). Here, the data was analysed using both clustering methods to account for potential differences in the microstates obtained using the different clustering methods.

Microstates in the delta (0–4 Hz), theta (4–8 Hz), alpha (8–13 Hz), and 2–20 Hz frequency bands were obtained after having filtered data in the respective frequency bands using a second-order Butterworth filter. For each frequency band, the following outputs were obtained for each patient,

- EEG scalp topographies when data is segmented into four microstates.
- The average number of times a microstate appears in a trial of EEG data.
- The average duration of each microstate in a trial.
- The average percentage of time spent in each microstate.

To achieve this, firstly four global microstates were obtained by pooling all patient data and clustering topographies to obtain the four microstates: *A*, *B*, *C* and *D*. Figure 2 shows global microstates obtained for patients in the two different outcome groups. We note that in our microstate analysis we use the same archetypal microstates (calculated by pooling data for both improved and unimproved conditions) which have the same general characteristics as those shown in Fig. 2 for classes A, B, C and D.

For each patient, the topographies at GFP maxima were then compared with each global microstate by computing squared correlation coefficients so as to disregard polarity.

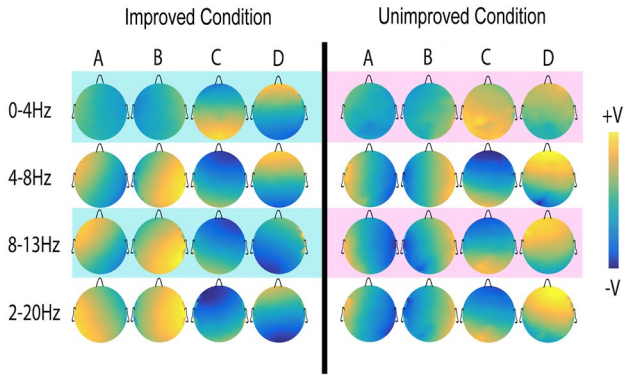

Fig. 2 Global microstate classes, *A*, *B*, *C* and *D*, obtained in the 0–4, 4–8, 8–13 and 0–20 Hz frequency bands, obtained globally for patients in the different outcome groups

Each topography was then assigned to a microstate class *A*, *B*, *C* or *D* dependent on the global microstate with which it best correlated, so that this process is much like a modified k-means clustering algorithm with the global maps as seed maps. The first spatial principal component was calculated for each microstate class to obtain four representative maps for each patient, which were then used in subsequent analyses.

For each patient, topographies at GFP maxima were compared to each microstate class by calculating squared correlation coefficients, and assigned to the class with which they best correlated. The average frequency, duration and percentage of time spent in each microstate were then determined, considering that EEG topographies remain stable between GFP minima as determined by previous research (Michel 2009). This procedure is illustrated in Fig. 3.

Entropy

Approximate Entropy

In order to be able to compare the *ApEn* of both patient groups we calculated *ApEn* with a short embedded dimension (m) template of 2, and a wide tolerance (r) and time delay (tau) equal to 0.2 × (standard deviation of data), as suggested by previous seminal research aiming to avoid the penalties associated with parameters lacking sufficient rigor (Pincus and Goldberger 1994; Pincus 1995; Bruhn et al. 2000; Pincus 2001). This approach has been adopted widely in EEG studies within and outside DOC research because such a normalization of r allows *ApEn* to remain "unchanged under uniform process magnification, reduction, or constant shift to higher or lower values" (Abásolo et al. 2005), which yields an *ApEn* unaffected by scale and translation (Ocak 2009; Sarà et al. 2011; Liang et al. 2015). *ApEn* was calculated separately for ten trials for each patient in

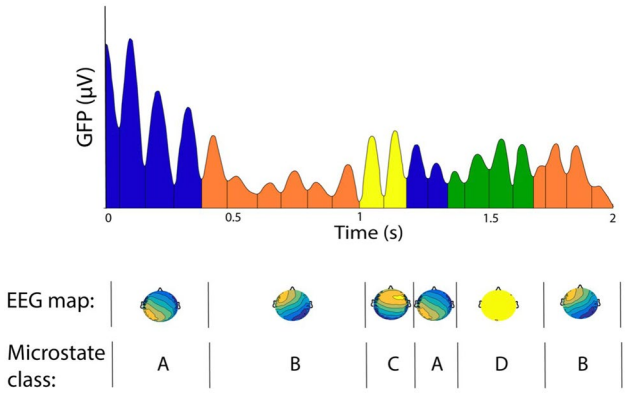

Fig. 3 The microstate analysis for one trial of data for one patient. Firstly, microstate classes, *A*, *B*, *C* and *D*, are obtained for each patient using a clustering algorithm, and then topographic maps at each time point are assigned to a microstate class. The different colours of the GFP curve represent the four microstate classes. The corresponding microstate topography at each time point, as well as the microstate class, are illustrated beneath the GFP curve

the delta, theta, alpha and beta (13–35 Hz) frequency bands for each channel. Furthermore, it is not within the scope of this paper to attempt to optimize various parameter values, but rather to explore existing quantitative methods in the way that they are currently implemented. Additionally, it is the comparison of the ApEn in the two different patient groups that is important (not the absolute value of ApEn) that is important in this study. These values were then averaged over the trials and over the channels to obtain a single descriptor as a feature in the classification scheme.

Permutation Entropy

We calculated permutation entropy over ten trials for each channel in the delta, theta, alpha and beta bands separately, using a time delay of one sample and an embedding dimension m of 3: Fig. 1 provides an illustration of the $3! = 6$ possible symbol representations of sub-vectors. Feature vectors for the classification scheme were obtained in a similar manner to those in the *ApEn* analysis.

Power in Alpha and Delta Frequency Bands

We obtained relative power values in the alpha and delta bands by computing the power in these bands as a fraction of the power across 1–50 Hz, which were then used as features in the classification scheme. We employed a multitaper method to overcome some of the limitations of conventional Fourier analysis. In principle, to describe a system in the frequency domain, an output sample of infinite length is needed. Moreover, infinitely many realisations of this output are needed to capture stochastic properties, which in most scenarios is not possible. Typically, the output is only observed as a single realisation with finite length, which often results in spectral estimates that are biased and exhibit high error variance (Babadi and Brown 2014).

To remedy this, we obtained several periodograms by multiplying the EEG signal with Slepian sequences, a family of mutually orthogonal tapers (windows), which additionally have optimal time–frequency concentration properties (Van De Ville et al. 2002) These periodograms (each one obtained using a different Slepian sequence as a window) were then averaged to produce the multitaper power spectral density estimate. Slepian sequences, $\hat{h}_n$, are defined as the eigenvectors of,

$$\sum_{n=0}^{N-1} \frac{\sin(2\pi W(m-n))}{\pi(m-n)} \hat{g}_n = \lambda \hat{g}_n \tag{9}$$

where N is the number of time samples of EEG data for one channel, and W is a half-bandwidth that defines a small frequency band centred around [1] f. Here, we chose [2] W of 0.002, and made use of the first 7 Slepian sequences based on the value of the corresponding eigenvalues.

Connectivity

Coherence

Magnitude-squared coherence and the imaginary part of coherence were calculated for each patient for each pair of electrodes in the delta, theta, alpha and beta frequency bands and averaged over 10 trials. [3] The median value of coherence for each electrode was then determined, and the mean of these median values used as a feature in the classification scheme.

Weighted Symbolic Mutual Information

To calculate wSMI, we transformed EEG data symbolically in the same way as has been described for the calculation of permutation entropy: data points are divided into subvectors of dimension m, with each element in the sub-vector separated by a fixed time delay, τ, similarly to the embedding performed for the calculation of permutation entropy. wSMI was calculated as described previously in the delta, theta, alpha and beta frequency bands with m of 3 and of 4, 8 and 32 time samples. These parameters were chosen based on the work of King et al. who first described the method (King et al. 2013). The authors note that different τ values are specific to different frequency bands, and note the importance of applying an appropriate low-pass filter before analysis to prevent aliasing. By band-pass filtering the signal, one can address the potential problem of aliasing as well as further

isolate the frequencies responsible of the wSMI differences across consciousness states.

Figure 1 shows the probability matrix used to calculate *wSMI* for an m of 3, and illustrates the $3! = 6$ possible symbol representations of sub-vectors. For each patient, wSMI was calculated over all electrode pairs and the median value determined for each trial. The median values for each of the ten trials were then averaged to obtain one value.

Symbolic Transfer Entropy

We transformed EEG data symbolically as described previously with an embedding dimension of $m = 3$ and time delay $\tau = 1$, and *TE* calculated for each patient in the delta, theta, alpha and beta frequency bands. Feature vectors were obtained by averaging *TE* over all electrodes and over 10 trials of data.

Complex Network Analysis

The present study makes use of non-directional binary links, which incorporates EEG results as shown in Fig. 4, such that a link is either present or absent depending on a threshold value of the connectivity measure.

We examined both average clustering coefficient and characteristic path length, with links between nodes determined by thresholding values for coherence between electrodes. Coherence in the delta, theta, alpha and beta ranges were thresholded at values of coherence of 0.8–0.95, incrementing by 0.01. We can thus define a binary link between two nodes if the magnitude-squared coherence between the two corresponding electrodes is above the threshold. If the threshold is too high, very few links between electrodes remain making it difficult to infer connectivity patterns, and if the threshold is too low very few differences in the connectivity graphs are present, making comparisons difficult. As noted in literature (Bordier et al. 2017), methods of determining? optimal? thresholds are widely discussed and researched, although it appears that no real consensus has been reached on how best to choose such thresholds. Thus, we observed empirically (on a different set of data) that 0.8–0.95 represented a broad enough range such that thresholds within this range represented a compromise between overly connected and overly sparse connectivity graphs.

Results

Obtained Participant Sample

As shown in Tables 1 and 2 we performed consciousness indexing with EEG data from 62 patients and predicted outcome with a subset of 39 patients, who had follow-up

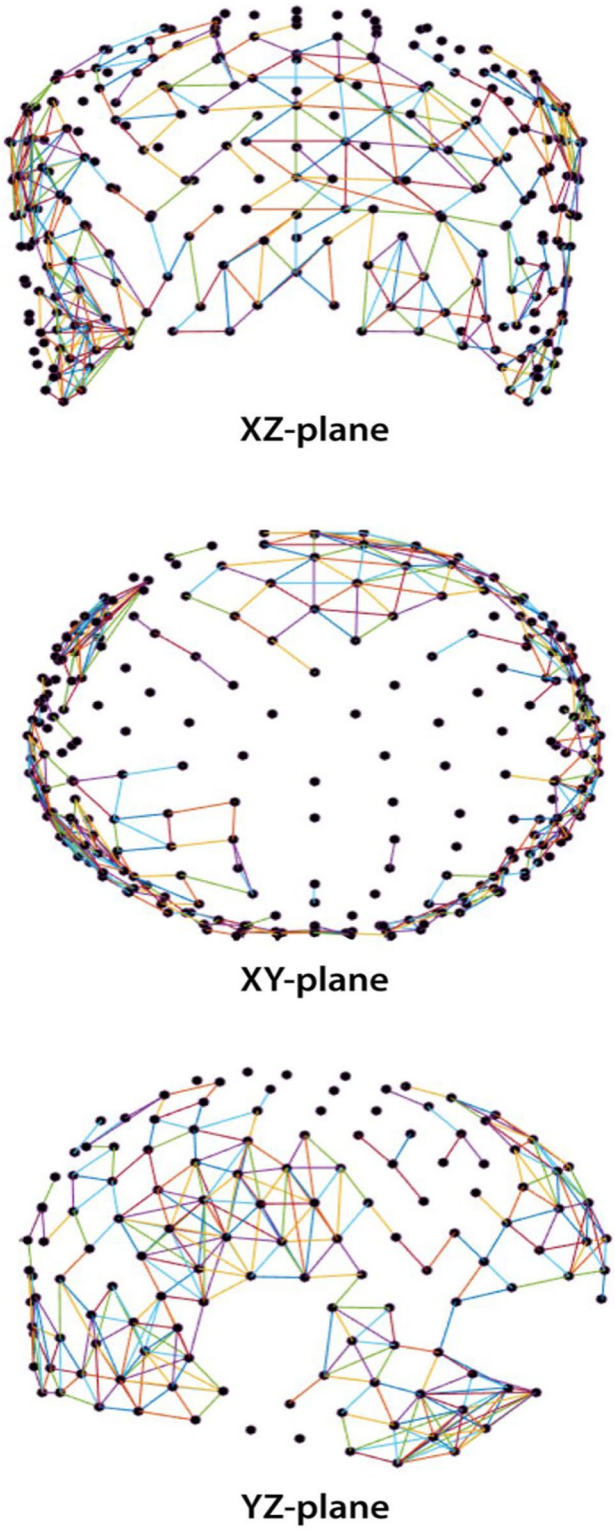

Fig. 4 A visualisation in the XZ-, XY- and YZ-planes of complex network analysis applied to EEG: this is an example of the network obtained for one patient when thresholding coherence in the beta range at 0.94. The nodes are represented by electrodes and binary non-directional links between two electrodes indicate a coherence of greater than 0.94 between those electrodes

Table 1 Characteristics of patients in the consciousness indexing group ($N = 62$)

Etiology	Age at admission in years	Gender		DOC category at baseline	
		M	F	UWS	MCS
Hypoxia	56.17 ± 14.08	17	12	28	1
TBI	39.71 ± 17.7	9	5	12	2
Ischemic stroke	47.00 ± 25.24	1	2	3	0
Brain tumor	74	0	1	0	1
ICH	62.33 ± 5.61	6	0	3	3
SAH	46.50 ± 9.59	3	5	4	4
Cerebral venous sinus thrombosis	25	0	1	1	0
Total	51.15 ± 16.42	36	26	51	11

EEG data. Mean time elapsed from baseline to follow-up was 589.26 ± 1125.32 days. Additional data on the obtained sample is available in the online resource.

Consciousness Indexing

Microstate

Percentage of time spent in microstate *D* in the alpha range ($AUC = 74 \pm 5\%, q < 0.0001$) was the best performing feature extracted at discriminating between MCS and UWS patients.

Entropy

ApEn in all frequency ranges was higher for MCS patients than UWS patients (delta: $AUC = 57 \pm 5\%$, $q < 0.01$, theta: $AUC = 55 \pm 2\%$, $q < 0.01$, alpha: $AUC = 57 \pm 5\%$, $q < 0.001$, beta: $AUC = 68 \pm 2\%$, $q < 0.001$). Permutation entropy in the alpha range was also significantly higher for MCS patients ($AUC = 61 \pm 2\%, q < 0.0001$).

Power in Alpha and Delta Frequency

Power in both the alpha frequencies was greater for MCS patients than UWS patients, and conversely for power in the delta frequencies. The measures performed similarly at distinguishing between UWS and MCS patients ($AUC = 54 \pm 3\%$, $q < 0.01$ for alpha range and $AUC = 58 \pm 7\%, q < 0.01$ for delta range).

Connectivity

Only imaginary coherence in the theta band yielded significant results. We found that coherence in the alpha and beta frequencies were higher for patients in UWS ($AUC = 64 \pm 4\%$, $q < 0.001$ in the alpha band and $AUC = 61 \pm 2\%, q < 0.001$ in the beta band). We also found that wSMI performed significantly in the theta range with t = 4 ($AUC = 60 \pm 3\%, q < 0.01$), the alpha range with t = 4 ($AUC = 56 \pm 4\%, q < 0.01$) and the delta range with t = 8 ($AUC = 69 \pm 1\%, q < 0.001$). Transfer entropy performed similarly in all frequency bands, with transfer entropy in the alpha band yielding the best results ($AUC = 67 \pm 3\%$, $q < 0.0001$).

Complex Network Analysis

We represented EEG signals as complex network graphs by thresholding coherence in the delta, theta, alpha and beta ranges, and found that both the characteristic path length and the clustering coefficient of these graphs successfully classified patients into UWS/MCS. The clustering coefficient of complex networks obtained by thresholding alpha coherence yielded reasonable classification accuracy on average ($AUC = 64 \pm 1\%$, $q < 0.001$), without the threshold having any significant effect. Similar results are obtained for

Table 2 Characteristics of patients in the outcome prediction subgroup ($N = 39$)

Etiology	Age at admission in years	Gender		DOC category at baseline		DOC category at follow-up			Time from admission to follow-up in days
		M	F	UWS	MCS	UWS	MCS	MCS+	
Hypoxia	56.95 ± 16.19	13	7	20	0	18	2	0	457.70 ± 824.21
TBI	42.88 ± 17.08	8	1	9	0	8	0	1	434.67 ± 796.26
Ischemic stroke	61.5 ± 3.54	1	1	2	0	1	0	1	32.00 ± 32.53
ICH	65.00 ± 4.24	3	0	3	0	1	1	1	386.00 ± 614.89
SAH	46.00 ± 1.41	0	4	4	0	1	1	2	165.75 ± 231.56
Cerebral venous sinus thrombosis	25	0	1	1	0	0	0	1	153
Total	51.85 ± 17.57	25	14	39	0	29	4	6	386.36 ± 717.06

average path length in the obtained by thresholding alpha coherence ($AUC = 65 \pm 4\%$, $q < 0.001$) and beta coherence ($AUC = 65 \pm 5\%$, $q < 0.001$). See Supplementary Figs. 1 and 2 for the distributions of clustering coefficients and path lengths with respect to state of consciousness.

Outcome prediction

Microstates

It appears that microstate *A* was particularly informative in predicting coma outcome. We found that the duration of microstate *A* in the delta band ($AUC = 75 \pm 5\%$, $q < 0.001$), the frequency of microstate *A* in the theta band ($AUC = 75 \pm 10\%$, $q < 0.01$), the percentage of time spent in microstate *A* in the theta band ($AUC = 85 \pm 2\%$, $q < 0.0001$) and the frequency of microstate *A* in the 2–20Hz band ($AUC = 73 \pm 3\%$, $q < 0.0001$) all perform significantly.

Entropy

ApEn in the alpha band efficiently predicted outcome ($AUC = 67 \pm 5\%$, $q < 0.001$), however permutation entropy performed better than *ApEn*: permutation entropy in the delta ($AUC = 71 \pm 5\%$, $q < 0.0001$), theta ($AUC = 83 \pm 3\%$, $q < 0.0001$) bands yielded promising results.

Power in the Alpha and Delta Frequency

Power in the alpha ($AUC = 64 \pm 4\%$, $q < 0.001$) and delta ($AUC = 68 \pm 9\%$, $q < 0.01$) performed better at discriminating outcome than indexing consciousness.

Connectivity

Coherence in the theta band yielded high classification accuracy ($AUC = 78 \pm 2\%$, $q < 0.0001$). Alpha ($AUC = 62 \pm 4\%$, $q < 0.001$) and beta coherence ($AUC = 67 \pm 1\%$, $q < 0.0001$) were also successful. Coherence in all frequency ranges was greater for patients who improved condition. Interestingly, only the imaginary part of coherence in the beta band achieved significant results ($AUC = 75 \pm 2\%$, $q < 0.0001$) and did not offer an advantage to magnitude-squared coherence as a classifier.

TE and *wSMI* also predicted patient outcome effectively. We found that TE was successful at predicting outcome both in the delta ($AUC = 70 \pm 3\%$, $q < 0.001$) and alpha band ($AUC = 78 \pm 3\%$, $q < 0.001$). We also found that *wSMI* in the alpha band with a time delay of 32 s ($AUC = 73 \pm 4\%$, $q < 0.0001$) exhibited the most notable prognostic power, but *wSMI* in the alpha band with $t = 8$ s ($AUC = 71 \pm 5\%$, $q < 0.001$) and in the delta band with $t = 8$ s ($AUC = 69 \pm 8\%$, $q < 0.001$) also yielded significant results.

Complex Network Analysis

We found that clustering coefficients, calculated from beta coherence ($AUC = 82 \pm 1\%$, $q < 0.0001$) and alpha coherence ($AUC = 82 \pm 2\%$, $q < 0.0001$) performed best at classifying patients into the two outcome categories, without the thresholds having much effect. Clustering coefficients in the theta (mean $AUC = 72 \pm 1\%$, $q < 0.0001$) range also exhibited significant results. However, path length did not show a strong association with outcome. Here, the two outcomes correspond to emergence from UWS to MCS, or death or a persistent DOC. See Supplementary Figs. 2 and 4 for the distributions of clustering coefficients and path lengths with respect to outcome.

Automated Outcome Prediction

We selected an optimal subset of features with SFFS for an automated outcome prediction scheme. To avoid selection bias, we apply feature selection to each fold within cross-validation and select the three features that are most represented to select features for a final model. A larger sample size, however, is needed to validate the robustness of these features as well as the risk of overfitting. It is our hope that this may at least demonstrate promise for approaches to EEG data analysis and coma studies that are grounded in quantification.

It consisted of the following three features: frequency of microstate A in the 2–20 Hz frequency band, path length obtained from thresholding alpha coherence, and clustering coefficient obtained from thresholding alpha coherence. Combining these features seemed to afford high prediction power ($AUC = 92 \pm 4\%$), as shown in Fig. 5.

Python and MATLAB toolboxes for the above calculations are freely available under the GNU public license for non-commercial use (https://qeeg.wordpress.com). Results are presented in greater detail in the online supplementary material.

Discussion

Most measures performed significantly better at predicting outcome of coma than at discriminating between UWS and MCS patients, indicating perhaps that the link between diagnosis and prognosis is not as compelling as originally thought, or perhaps that some patients had been erroneously classified, considering that in clinical practice misdiagnoses occur in up to 43% of cases, especially when an inappropriate behavioural scale is used (Schnakers et al.

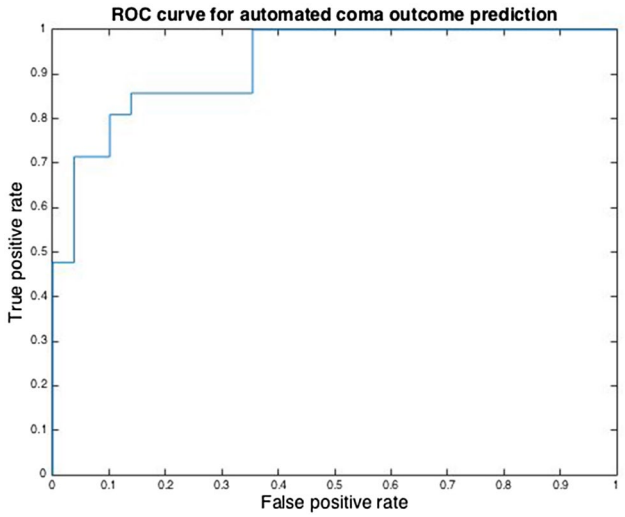

Fig. 5 ROC curve showing the performance of the combination of the three features selected using *SFFS*, namely the frequency of microstate A in the 2–20 Hz frequency band, path length obtained from thresholding alpha coherence and clustering coefficient obtained from thresholding alpha coherence

2009). Additionally, these strictly-defined categories do not take into account that UWS patients may actually be minimally or even fully conscious (van Erp et al. 2015). As mentioned, we found that all connectivity measures were not significantly different for UWS and MCS patients, although many of these metrics were greater in UWS patients than MCS patients. This is in direct contrast to previous research on *wSMI* and *TE* which indicates that measures of connectivity systematically increase with degree of consciousness, although in previous work auditory paradigm data was analysed whereas resting-state data was used in the present study (King et al. 2013; Thul et al. 2016). We did however find greater *wSMI*, *TE* and coherence (in all frequency ranges) in patients with improved outcome than those with unimproved outcome, indicating possible power of connectivity measures in prognosis instead of diagnosis.

Similarly, Lehembre et al. (2012) found that patients in UWS had significantly lower coherence than MCS patients in the theta and alpha bands. We did also observe this relationship, but the result was not significant. However, in a more recent study, Schorr et al. (2016) found that coherence could not be used to differentiate UWS and MCS patients, but could instead predict the recovery of UWS to MCS. The present study however did not find significant differences in the coherence between patients with improved and unimproved condition. This may be a consequence of averaging the coherence across all parts of the brain instead of investigating the connectivity between different parts of the brain separately, as was done by Schorr et al. (2016).

There were however significant differences between entropy of MCS and UWS patients, with permutation entropy and *ApEn* significantly higher in MCS patients, in accordance with the previous findings (Thul et al. 2016; Gosseries et al. 2011). Similarly, we found that patients with improved outcome exhibited greater EEG entropy than those with unimproved outcomes. It is hypothesised that the increased entropy is reflective of the increased complexity of neural networks that are necessary to support consciousness.

Power in the alpha band was greater for MCS patients than for UWS patients, and delta power was greater for UWS patients compared to MCS patients as also found by Lehembre et al. (2012), although the differences were not significant. The power in the delta band, however, was significantly smaller for patients who improved condition.

Our analysis of the topologies of the different patient groups largely agrees with the findings presented in the study by Chennu et al., and we highlight their work in comparing EEG-based connectivity hubs to PET data and glucose metabolism itself (Chennu et al. 2017). They show that these measures of connectivity correlate with the potential physiological underpinnings of consciousness, which may help to explain the relatively high performance of these measures at predicting outcome. Like in their work, we find that patients who improved condition exhibited greater connectivity, indicated by higher average clustering coefficients, and shorter characteristic path lengths (see Supplementary Figures).

We also draw attention to work by Sitt et al. which similarly to this study aimed to perform a large-scale analysis of the EEG measures in discriminating UWS and MCS patients (Sitt et al. 2014). This study complements much of this work, and further demonstrates differences in EEG features in predicting outcome as opposed to indexing consciousness.

Collectively, the comparison between these results seems to indicate that the results are dependent on the type of paradigm used, and possibly various other specific parameters used in calculations, like the length of each trial. It is also interesting to note that the number of electrodes used in this study is significantly higher than those used in many previous studies, providing information at more locations across the scalp, potentially allowing for more robust results. This is by virtue of the fact that high channel-density recordings may provide information from more regions of the brain (and thus more reflective of overall brain dynamics) than low channel-density recordings, as well as by providing more data over the same period of time.

With regards to the microstate analysis, we found a very pronounced difference in the percentage of time spent in microstate *D* in the alpha frequency in the two patient groups with respect to outcome, with patients with unimproved outcome spending more time in microstate *D*. It is possible that each microstate reflects an underlying neurological function,

as activity of different neural populations is responsible for the different landscapes of electrical potentials characterized by each microstate (Lehmann et al. 2006) This possibly indicates that improved outcome patients spend more time on other neurological tasks (represented by the other microstates) than unimproved outcome patients.

While effective and accurate, it is questionable whether the methods and measures studied here may perform sufficiently well to replace current practice for prognosticating coma on an individual basis. However, the automatic classification scheme is simple and cost-effective to implement and may indeed provide supplemental information to better inform medical practitioners when assessing prognosis. Moreover, the results of this study may not only be useful in clinical practice, but also in better understanding the nature of consciousness and the roots of disorders of consciousness. However, an important goal of the present study was to investigate several EEG biomarkers of consciousness on the same dataset to be able to compare the relative usefulness of these features. Most features presented here are commonly applied in EEG analyses of consciousness, but it has remained unclear how they perform comparatively. We also aimed to apply measures that are ordinarily applied to index consciousness to instead predict outcome, thus avoiding the problem of misdiagnoses.

Recent theories attribute disorders of consciousness to the disconnection of different cortical networks, rather than the dysfunction of a single area of the brain (Ovadia-Caro et al. 2012; Vanhaudenhuyse et al. 2010). For this reason, it may be important to investigate the network structures and motifs underlying consciousness and their interconnectedness through measures of functional connectivity, like those explored in this study. It is possible that disorders of consciousness stem from a functional isolation within the cerebral cortex, due to a derangement of neural networks and a consequent decrease in connectivity. The measures of connectivity, entropy and graph-theoretical statistics investigated here directly assess the degree of functional isolation through the investigation of the interconnectedness of subdivisions within the neural networks, as well as the complexity of these neural networks through the quantification of the unpredictability of its outputs. While the measures studied here do support this proposed theory of consciousness to some extent, it is entirely possible that other measures may better reflect true brain interactions, and consequently be more successful at interrogating differences between positive and negative outcome patients. It is thus necessary to continue to propose EEG methods to accurately reveal interactions between different cortical networks, and compare the results to those from other brain imaging methods, such as fMRI. These new methods of analysis may then firstly contribute additional evidence to the leading theory or otherwise, and secondly prove to be more useful in prognosticating coma than the methods studied here.

Conclusion

Our results suggest that several mathematically precise biomarkers perform significantly better than expected by chance at predicting outcome of coma, with the most promising results obtained through the analysis of EEG signals represented as microstates. These series of sequential topographies of electrical fields possibly provide insight into the differences between UWS and MCS patients, as well as key differences between patients with improved and unimproved outcomes. As far as we know, microstate analysis had not previously been applied to outcome prediction in this manner, such that this study is the first indication of the potential promise of this method.

An important goal of the study was to investigate several EEG biomarkers of consciousness on the same dataset to be able to compare the relative usefulness of these features. Most features presented here are commonly applied in EEG analyses of consciousness, but it has remained unclear how they perform comparatively. We also aimed to apply measures that are ordinarily applied to index consciousness to instead predict outcome, thus avoiding the problem of misdiagnoses.

Lastly, we aimed to design an automated classification scheme using SFFS: we found that combining metrics such frequency of microstate A in the 2–20 Hz frequency band, path length obtained from thresholding alpha coherence, and clustering coefficient obtained from thresholding alpha coherence affords high prediction power with an *AUC* of $92 \pm 4\%$. While this may still not be ideal for prognostication of individuals, it may indeed serve to better inform medical practitioners when assessing prognosis.

Acknowledgements The authors wish to thank patients and their caregivers as well as the Information and Communication Technology High Performance Computing Team of the University of Cape Town. Part of this study was supported by Grant 2011013 of the Hannelore-Kohl-Stiftung, and the Deutsche Stiftung Neurologie.

Compliance with Ethical Standards

Conflict of interest The authors declare that they have no conflict of interest.

Ethical Approval All procedures performed in the present study involving human participants were approved by the institutional review board of the University of Munich and were in accordance with the ethical standards of the 1964 Helsinki declaration and its later amendments.

References

Babadi B, Brown EN (2014) A review of multitaper spectral analysis. IEEE Trans Biomed Eng 61:1555–1564. https://doi.org/10.1109/TBME.2014.2311996

Barnett L, Barrett AB, Seth AK (2009) Granger causality and transfer entropy are equivalent for Gaussian variables. Phys Rev Lett 103:238701. https://doi.org/10.1103/PhysRevLett.103.238701

Blume C, Del Giudice R, Wislowska M et al (2015) Across the consciousness continuum-from unresponsive wakefulness to sleep. Front Hum Neurosci 9:105. https://doi.org/10.3389/fnhum.2015.00105

Bordier C, Nicolini C, Bifone A (2017) Graph analysis and modularity of brain functional connectivity networks: searching for the optimal threshold. arXiv preprint arXiv:1705.0648

Brodbeck V, Kuhn A, von Wegner F et al (2012) EEG microstates of wakefulness and NREM sleep. NeuroImage 62:2129–2139. https://doi.org/10.1016/j.neuroimage.2012.05.060

Bruhn J, Rpcke H, Hoeft A (2000) Approximate entropy as an electroencephalographic measure of anesthetic drug effect during desflurane anesthesia. Anesthesiology 92:715–726

Chennu S et al (2017) Brain networks predict metabolism, diagnosis and prognosis at the bedside in disorders of consciousness. Brain 140(8):2120–2132

Daw CS, Finney CEA, Tracy ER (2003) A review of symbolic analysis of experimental data. Rev Sci Instrum 74:915–930. https://doi.org/10.1063/1.1531823

Giacino JT, Ashwal S, Childs N et al (2002) The minimally conscious state: definition and diagnostic criteria. Neurology 58:349–353

Giacino JT, Fins JJ, Laureys S, Schiff ND (2014) Disorders of consciousness after acquired brain injury: the state of the science. Nat Rev Neurol 10:99–114. https://doi.org/10.1038/nrneurol.2013.279

Gosseries O, Schnakers C, Ledoux D et al (2011) Automated EEG entropy measurements in coma, vegetative state/unresponsive wakefulness syndrome and minimally conscious state. Funct Neurol 26:25–30

Graf J, Mhlhoff C, Doig GS et al (2008) Health care costs, long-term survival, and quality of life following intensive care unit admission after cardiac arrest. Crit Care 12:R92. https://doi.org/10.1186/cc6963

Grill E, Klein A-M, Howell K et al (2013) Rationale and design of the prospective German registry of outcome in patients with severe disorders of consciousness after acute brain injury. Arch Phys Med Rehab 94:1870–1876. https://doi.org/10.1016/j.apmr.2012.10.040

Howell K, Grill E, Klein A-M et al (2013) Rehabilitation outcome of anoxic-ischaemic encephalopathy survivors with prolonged disorders of consciousness. Resuscitation 84:1409–1415. https://doi.org/10.1016/j.resuscitation.2013.05.015

Kannathal N, Choo ML, Acharya UR, Sadasivan PK (2005) Entropies for detection of epilepsy in EEG. Comput Methods Progr Biomed 80:187–194. https://doi.org/10.1016/j.cmpb.2005.06.012

King J-R, Sitt JD, Faugeras F et al (2013) Information sharing in the brain indexes consciousness in noncommunicative patients. Curr Biol 23:1914–1919. https://doi.org/10.1016/j.cub.2013.07.075

Koenig T, Melie-Garca L (2010) A method to determine the presence of averaged event-related fields using randomization tests. Brain Topogr 23:233–242. https://doi.org/10.1007/s10548-010-0142-1

Kondziella D, Friberg CK, Frokjaer VG et al (2016) Preserved consciousness in vegetative and minimal conscious states: systematic review and meta-analysis. J Neurol Neurosurg Psychiatry 87:485–492. https://doi.org/10.1136/jnnp-2015-310958

Kuhn A, Brodbeck V, Tagliazucchi E et al (2015) Narcoleptic patients show fragmented EEG-microstructure during early NREM sleep. Brain Topogr 28:619–635. https://doi.org/10.1007/s10548-014-0387-1

Laureys S, Celesia GG, Cohadon F et al (2010) Unresponsive wakefulness syndrome: a new name for the vegetative state or apallic syndrome. BMC Med 8:68. https://doi.org/10.1186/1741-7015-8-68

Lee U, Blain-Moraes S, Mashour GA (2015) Assessing levels of consciousness with symbolic analysis. Philos Trans A 373(2034):20140117. https://doi.org/10.1098/rsta.2014.0117

Lehembre R, Marie-Aurlie B, Vanhaudenhuyse A et al (2012) Resting-state EEG study of comatose patients: a connectivity and frequency analysis to find differences between vegetative and minimally conscious states. Funct Neurol 27:41–47

Lehmann D, Faber PL, Gianotti LR et al (2006) Coherence and phase locking in the scalp EEG and between LORETA model sources, and microstates as putative mechanisms of brain temporo-spatial functional organization. J Physiol 99(1):29–36

Lehmann D, Faber PL, Galderisi S et al (2005) EEG microstate duration and syntax in acute, medication-naive, first-episode schizophrenia: a multi-center study. Psychiatry Res 138:141–156. https://doi.org/10.1016/j.pscychresns.2004.05.007

Lehmann D, Ozaki H, Pal I (1987) EEG alpha map series: brain microstates by space-oriented adaptive segmentation. Electroencephalogr Clin Neurophysiol 67:271–288

Lehmann D, Strik WK, Henggeler B et al (1998) Brain electric microstates and momentary conscious mind states as building blocks of spontaneous thinking I: visual imagery and abstract thoughts. Int J Psychophysiol 29:1–11

Liang Z, Wang Y, Sun X et al (2015) EEG entropy measures in anesthesia. Front Comput Neurosci 9:16. https://doi.org/10.3389/fncom.2015.00016

Lopez-Rolon A, Bender A (2015) Hypoxia and Outcome Prediction in Early-Stage Coma (Project HOPE): an observational prospective cohort study. BMC Neurol 15:82. https://doi.org/10.1186/s12883-015-0337-x

Mason SJ, Graham NE (2002) Areas beneath the relative operating characteristics (ROC) and relative operating levels (ROL) curves: statistical significance and interpretation. Q J R Meteorol Soc 128:2145–2166. https://doi.org/10.1256/003590002320603584

Michel CM (2009) Electrical neuroimaging. Cambridge University Press, Cambridge

Murray MM, Brunet D, Michel CM (2008) Topographic ERP analyses: a step-by-step tutorial review. Brain Topogr 20:249–264. https://doi.org/10.1007/s10548-008-0054-5

Noirhomme Q, Laureys S (2014) Consciousness and unconsciousness: an EEG perspective. Clin EEG Neurosci 45:4–5. https://doi.org/10.1177/1550059413519518

Noirhomme Q et al (2015) Look at my classifier's result?: disentangling unresponsive from (minimally) conscious patients. Neuroimage 145:288–303

Nunez PL, Srinivasan R, Westdorp AF et al (1997) EEG coherency I: statistics, reference electrode, volume conduction, Laplacians, cortical imaging, and interpretation at multiple scales. Clin Neurophysiol 103:499–515

Ocak H (2009) Automatic detection of epileptic seizures in EEG using discrete wavelet transform and approximate entropy. Expert Syst Appl 36(2):2027–2036. https://doi.org/10.1016/j.eswa.2007.12.065

Ovadia-Caro S, Nir Y, Soddu A et al (2012) Reduction in inter-hemispheric connectivity in disorders of consciousness. PLoS ONE 7:e37238. https://doi.org/10.1371/journal.pone.0037238

Pascual-Marqui RD, Michel CM, Lehmann D (1995) Segmentation of brain electrical activity into microstates: model estimation and validation. IEEE Trans Biomed Eng 42:658–665. https://doi.org/10.1109/10.391164

Pincus SM (1995) Approximate entropy (ApEn) as a complexity measure. Chaos 5:110–117. https://doi.org/10.1063/1.166092

Pincus SM (2001) Assessing serial irregularity and its implications for health. Ann N Y Acad Sci 954:245–267

Pincus SM, Goldberger AL (1994) Physiological time-series analysis: what does regularity quantify? Am J Physiol 266:H1643–1656

Pincus S, Singer BH (2014) Higher-order dangers and precisely constructed taxa in models of randomness. Proc Nat Acad Sci 111(15):5485–5490. https://doi.org/10.1073/pnas.1402621111

Posner JB, Saper CB, Schiff N, Plum F (2007) Plum and posner's diagnosis of stupor and coma, 4th edn. Oxford University Press, Oxford

Sarà M, Pistoia F, Pasqualetti P et al (2011) Functional isolation within the cerebral cortex in the vegetative state: a nonlinear method to predict clinical outcomes. Neurorehabilit Neural Repair 25:35–42. https://doi.org/10.1177/1545968310378508

Schnakers C, Vanhaudenhuyse A, Giacino J et al (2009) Diagnostic accuracy of the vegetative and minimally conscious state: clinical consensus versus standardized neurobehavioral assessment. BMC Neurol 9:35. https://doi.org/10.1186/1471-2377-9-35

Schorr B, Schlee W, Arndt M et al (2015) Stability of auditory event-related potentials in coma research. J Neurol 262:307–315. https://doi.org/10.1007/s00415-014-7561-y

Schorr B, Schlee W, Arndt M, Bender A (2016) Coherence in resting-state EEG as a predictor for the recovery from unresponsive wakefulness syndrome. J Neurol 263:937–953. https://doi.org/10.1007/s00415-016-8084-5

Sitt JD et al (2014) Large scale screening of neural signatures of consciousness in patients in a vegetative or minimally conscious state. Brain 137.8:2258–2270

Stender J, Gjedde A, Laureys S (2015) Detection of consciousness in the severely injured brain. In: Vincent J-L (ed) Annual update in intensive care and emergency medicine 2015. Springer, Cham, pp 495–506

Thul A, Lechinger J, Donis J et al (2016) EEG entropy measures indicate decrease of cortical information processing in disorders of consciousness. Clin Neurophysiol 127(2):1419–1427

Van De Ville D, Philips W, Lemahieu I (2002) On the n-dimensional extension of the discrete prolate spheroidal window. IEEE Signal Process Lett 9:89–91

van Erp WS, Lavrijsen JCM, Vos PE et al (2015) The vegetative state: prevalence, misdiagnosis, and treatment limitations. J Am Med Dir Assoc 16:85.e9–85.e14. https://doi.org/10.1016/j.jamda.2014.10.014

Vanhaudenhuyse A, Noirhomme Q, Tshibanda LJ-F et al (2010) Default network connectivity reflects the level of consciousness in non-communicative brain-damaged patients. Brain J Neurol 133:161–171. https://doi.org/10.1093/brain/awp313

Ververidis D, Kotropoulos C (2008) Fast and accurate sequential floating forward feature selection with the Bayes classifier applied to speech emotion recognition. Signal Process 88(12):2956–2970. https://doi.org/10.1016/j.sigpro.2008.07.001